Science of Remote Sensing 5 (2022) 100056

Contents lists available at ScienceDirect

Science of Remote Sensing

journal homepage: www.sciencedirect.com/journal/science-of-remote-sensing

Following the cosmic-ray-neutron-sensing-based soil moisture under grassland and forest: Exploring the potential of optical and SAR remote sensing

Veronika Döpper [a], Thomas Jagdhuber [b,c], Ann-Kathrin Holtgrave [a,d], Maik Heistermann [e], Till Francke [e], Birgit Kleinschmit [a], Michael Förster [a,*]

[a] Technische Universität Berlin, Institute for Landscape Architecture and Environmental Planning, Geoinformation in Environmental Planning Lab, Straße des 17. Juni 145, 10623 Berlin, Germany
[b] German Aerospace Center, Microwaves and Radar Institute, Münchener Strasse 20, 82234 Wessling, Germany
[c] Augsburg University, Institute of Geography, Alter Postweg 118, 86159, Germany
[d] Johann Heinrich von Thünen-Institute, Federal Research Institute for Rural Areas, Forestry and Fisheries, Bundesallee 64, 38116 Brunswick, Germany
[e] University of Potsdam, Institute of Environmental Science and Geography, Karl-Liebknecht-Straße 24–25, 14476 Potsdam, Germany

ARTICLE INFO

Keywords:
Sentinel 1
Sentinel 2
Soil texture
Topography
Sensing volume
Random forest regression
CRNS

ABSTRACT

Deriving soil moisture content (SMC) at the regional scale with different spatial and temporal land cover changes is still a challenge for active and passive remote sensing systems, often coped with machine learning methods. So far, the reference measurements of the data-driven approaches are usually based on point data, which entails a scale gap to the resolution of the remote sensing data. Cosmic Ray Neutron Sensing (CRNS) indirectly provides SMC estimates of a soil volume covering more than 1 ha and vertical depth up to 80 cm and is thus able to narrow this scale gap. So far, the CRNS-based SMC has only been used as validation source of remote sensing based SMC products. Its beneficial large sensing volume, especially in depth, has not been exploited yet. However, the sensing volume of the CRNS, which is changing with hydrological conditions, bears challenges for the comparison with remote sensing observations. This study, for the fist time, aims to understand the direct linkage of optical (Sentinel 2) and SAR (Sentinel 1) data with CRNS-based SMC. Thereby, the CRNS-based SMC is obtained by an experimental CRNS cluster that covers the high temporal and spatial SMC variability of an entire pre-alpine subcatchment. Using different Random Forest regressions, we analyze the potentials and limitations of both remote sensing sensors to follow the CRNS-based SMC signal. Our results show that it is possible to link the CRNS-based SMC signal with SAR and optical remote sensing observations via Random Forest modelling. We found that Sentinel 2 data is able to separate wet from dry periods with a R^2 of 0.68. It is less affected by the changing soil volume that contributes to the CRNS-based SMC signal and it is able to assign a land cover specific SMC distribution. However, Sentinel 2 regression models are not accurate ($R^2 < 0.21$) in mapping the CRNS-based SMC for the frequently mowed grassland areas of the study site. It requires soil type and topographical information to accurately follow the CRNS-based SMC signal with Random Forest regression. Sentinel 1 data instead is affected by the changing soil volume that contributes to the CRNS-based SMC signal. It has reasonable model performance ($R^2 = 0.34$) when the CRNS data correspond to surface SMC. Also for Sentinel 1 the retrieval is impacted by the mowing activities at the test site. When separating the CRNS data set into dry and wet periods, soil properties and topography are the main drivers of SMC estimation. Sentinel 1 or Sentinel 2 data add the existing temporal variability to the regression models. The analysis underlines the need of combining optical and SAR observations (Sentinel 1, Sentinel 2) as well as soil property and topographical information to understand and follow the CRNS-based SMC signal for different hydrological conditions and land cover types.

* Corresponding author. Straße des 17. Juni 145, Office: EB 5, 10623, Berlin, Germany.
E-mail address: michael.foerster@tu-berlin.de (M. Förster).

https://doi.org/10.1016/j.srs.2022.100056
Received 16 November 2021; Received in revised form 26 February 2022; Accepted 8 May 2022
Available online 13 May 2022

1. Introduction

Soil moisture content (SMC) is a key variable of land-atmosphere interactions: It controls the exchange of water and energy at the soil-atmosphere boundary, thus influencing evaporation and precipitation (Yang et al., 2018), runoff characteristics (Ghajarnia et al., 2020) and water availability for vegetation (Porporato et al., 2001). The accurate information on spatial and temporal states of soil moisture are therefore important for a broad range of applications, such as drought monitoring (Lu et al., 2021), crop yield estimation (Holzman et al., 2018) or flood forecasting (Massari et al., 2018).

Remote sensing approaches using active and passive microwaves (Edokossi et al., 2020; Bauer-Marschallinger et al., 2019; Vergopolan et al., 2021), thermal and optical data (Li et al., 2021; Zhang and Zhou, 2016) have demonstrated distinct capabilities to map SMC at different spatial resolutions and soil depths (Kumar et al., 2021; Peng et al., 2021) from the field (Ma et al., 2020; Vergopolan et al., 2021) to the global scale (Kumar et al., 2021; Mohanty et al., 2017; Li et al., 2021). Despite the multitude of remote sensing approaches, the retrieval of SMC at the root zone at high spatial and temporal resolutions remains a key challenge (Peng et al., 2021).

When aiming for SMC products with a spatial resolution of <100 m, data driven approaches using high-resolution optical, e.g. the MSI sensor of Sentinel 2 (S2) (Liu et al., 2020, 2021; Zaman et al., 2012), or active microwave sensors, e.g. the SAR mounted on Sentinel 1 (S1) (Hänsch et al., 2020; Holtgrave et al., 2018; Pasolli et al., 2014), provide satisfactory results. Extensive research has shown that these machine-learning-based retrievals of SMC highly benefit from time-invariant information on topography and soil properties (Sedaghat et al., 2022; Holtgrave et al., 2018; Liu et al., 2012; Pasolli et al., 2015; Schnur et al., 2010).

However, the ground reference data of the remotely-based SMC retrievals are, in most cases, point-scale measurements (Sedaghat et al., 2022; Ambrosone et al., 2020; Liu et al., 2021; El Hajj et al., 2019; Holtgrave et al., 2018; Vergopolan et al., 2021). The scale gap between the remote sensing and in-situ (point) measurements unavoidably leads to inaccuracies due to the missing spatial coverage of the in-situ data compared to satellite remote sensing acquisitions (Crow et al., 2005; Gruber et al., 2020).

Cosmic Ray Neutron Sensing (CRNS) (Zreda et al., 2008) reduces this scale mismatch. The CRNS method estimates SMC in a non-invasive and temporally continuous way within a footprint radius ≥130 m and a varying vertical depth of 15–83 cm (Köhli et al., 2015). The method is based on monitoring the density of fast neutrons, which are produced by high-energetic neutron showers generated by cosmic-rays entering the atmosphere. Since the fast neutrons are moderated primarily by hydrogen, their count rates are inversely correlated with the amount of hydrogen in the environment surrounding the CRNS probe. Hydrogen is prevalent in natural soils, making the changes in fast neutron count rates mainly governed by variations in the SMC (Zreda et al., 2008).

Since the development of the CRNS method, considerable knowledge on the signal interpretation (Köhli et al., 2015, 2021; Jakobi et al., 2018), sensor calibration (Schrön et al., 2017; Scheiffele et al., 2020), data processing (Power et al., 2021) and sensor uncertainties (Iwema et al., 2021; Baroni et al., 2018) has been assembled as well as mobile versions developed (Desilets et al., 2010; Schrön et al., 2018, 2021). This is expressed in an increasing number of applications of the CRNS-based SMC in a variety of research disciplines (Barbosa et al., 2021; Dimitrova-Petrova et al., 2020; Patil et al., 2021; Franz et al., 2020). In the field of remote sensing, the CRNS-based SMC is used primarily to validate developed near surface SMC products (Duygu and Akyürek, 2019; Howells et al., 2021; Montzka et al., 2017; Ma et al., 2020; Fersch et al., 2018). The beneficial large sensing volume, which also covers the root zone SMC, has not been fully exploited yet. This can be achieved via a data-driven linkage with remote sensing observations. Besides its sensing volume, the large data amount created by novel adaptations of the CRNS method make it an appealing ground reference measurement for the data-driven linkage with remote sensing observations.

Analysis using CRNS-based SMC as validation measurement of high-resolution SAR-based SMC products reveal a vertical and horizontal sensing mismatch between the CRNS and SAR sensors, impacting the comparability of the retrieved product with CRNS-based SMC (Ma et al., 2020; Fersch et al., 2018; Bayat et al., 2020). These results indicate that one of the greatest challenges of a direct linkage of remote sensing observations with CRNS-based SMC are the different vertical sensing depths of remote sensing observations and CRNS.

Optical remote sensing is able to retrieve SMC of the skin layer of bare soil based on changes in soil brightness with changing SMC (Liu et al., 2020; Bablet et al., 2018). For vegetated areas, in turn, SMC at the root zone can be derived (Liu et al., 2021; Wyatt et al., 2021; Sadeghi et al., 2017) using the link between plant traits, such as leaf water content or chlorophyll content, and SMC at depths where major water uptake takes place (Bollig and Feller, 2014; Gross et al., 2008). A considerable amount of literature has been published on the successful mapping of these SMC relevant plant traits (Lei et al., 2022; Xie et al., 2019; Zhao and Qin, 2019; Zhang et al., 2018) and SMC itself using optical remote sensing (Döpper et al., 2022; Liu et al., 2020, 2021; West et al., 2018; Sadeghi et al., 2017; Hassan-Esfahani et al., 2017; Zaman et al., 2012).

Instead of using proxies for the retrieval of SMC, active microwave remote sensing uses the increase of the dielectric constant of the soil medium with wetting as a direct link to the observed water body. This and the denser time series makes it the more common remote sensing sensor in the field of remote sensing of SMC. The penetration depth of the microwaves depends on wavelength, acquisition characteristics such as incidence angle and polarization (Baghdadi et al., 2017; Ulaby et al., 2014) as well as site characteristics such as SMC and land cover (Baghdadi et al., 2017; El Hajj et al., 2019). For the C-band wavelength, which is also used for S1, simulations and correlation analyses report a penetration depth of the first centimeters of the soil layer when no vegetation is present (Nolan and Fatland, 2003; Owe and Van de Griend, 1998; Ulaby et al., 2014).

The CRNS sensing volume, in turn, dynamically changes with varying amount of hydrogen in the environment. The higher the amount of hydrogen in the soil, the lower the footprint extent in horizontal and vertical scale (Desilets et al., 2010; Köhli et al., 2015; Zreda et al., 2008).

Given these differences in sensing depth, a systematic analysis of the implications for linking remote sensing observations with CRNS-based SMC is needed before large-scale applications are envisioned. The recently published dataset by Fersch et al. (2020b), which for the first time covers an entire sub-catchment with CRNS stations, is ideally suited for such a preliminary analysis. The spatially dense distribution of CRNS measurements and the small extent of the catchment area allow a controlled exploration of the factors influencing the data-driven modelling of CRNS-based SMC. In this regard, the study aims to provide initial insights for the development of a novel regional SMC product based on CRNS with the following research questions:

i) Is it possible to follow the CRNS-based SMC using a machine learning-based synergy of S1, S2 and site-specific (topography and soil) information?
ii) Do the distinct sensing volumes of the different remote sensing observations and the CRNS affect the quality of a data-driven modelling of CRNS-based SMC?
iii) What kind of information from remote sensing and test site characteristics is needed for following the CRNS-based SMC signal?

2. Methods and data

2.1. Fendt site

The Fendt site, as shown in Fig. 1, is part of the Pre-Alpine Terrestrial Environmental Observatory (TERENO, Kiese et al., 2018) and is located in the Rott headwater catchment (approx. 595 m ASL), about 50 km southwest of Munich, Bavaria, Germany.

As can be seen from Fig. 1b, the land cover of the headwater catchment consists mainly of intensively managed grassland (Kiese et al., 2018). A temperate forest, heterogeneous in species and age, covers the eastern slope. Towards the side slopes of the shallow valley gravels mixed with loamy and silty fractions are predominant. At the lower elevations soil texture comprises mainly silty and loamy sediments with peaty compositions towards the draining rivulet (Fersch et al., 2018). For further details on the site the reader is referred to Fersch et al. (2020b, 2018) and Kiese et al. (2018).

2.2. Soil moisture content data

This analysis relies on an unique data set of CRNS-based SMC that covers the spatial and temporal heterogeneities of SMC across an entire sub-catchment. The data set thus encompasses the spatio-temporal SMC dynamics associated with different land cover types, topographic settings, and soil properties during a period of ponding until the subsequent dry-down of the soils. It comprises SMC estimates of 17 stationary CRNS probes distributed within the Fendt site as part of a dense sensor network (Fig. 1d), operating from May 5, 2019 to July 22, 2019 (Fersch et al., 2020a). An additional CRNS probe served as standardization of the neutron count rates of the different sensors (Fersch et al., 2020b). We corrected the standardized neutron count rates for the effects of incoming cosmic neutron flux, barometric pressure, and atmospheric water vapor as summarized by Andreasen et al. (2017). The necessary input data for these corrections originate from the meteorological station of the TERENO test site (Fersch et al., 2020a) and the neutron monitor data at Jungfraujoch (Neutron Monitor Database, 2019). We accounted for the effect of vegetation on the neutron count rates by following Baatz et al. (2015) using biomass samples and estimates of the grassland and forest areas (Fersch et al., 2020a; Stockmann, 2020). To decrease the noise in the data, an unweighted 24 h rolling average was applied, maintaining the 20 min temporal resolution of the measurements.

The corrected and smoothed neutron count rates were calibrated with manually sampled soil moisture data (Fersch et al., 2020a). For computing the average observed SMC in a CRNS probe footprint, an iterative horizontal and vertical weighting procedure as described in Schrön et al. (2017) was applied. The time series of SMC based on the calibrated neutron count rates was produced by applying the transfer function as proposed by Desilets et al. (2010). Further details on the manually sampled SMC and biomass data as well as the correction and calibration procedure can be found in Fersch et al. (2020b) and Heistermann et al. (2021).

For the vertical interpretation of the CRNS-based SMC signal, we used SMC measurements of the SoilNet (Fersch et al., 2020a), deployed in 2015 in the north-western part of the Fendt site (see Fig. 1). We computed a weighted average after Schrön et al. (2017) of all nodes within a radius of 45 m of CRNS probes #3, #8, #17, #18 and #25 at a depth of 5 cm and 20 cm. This comparison revealed that the second half

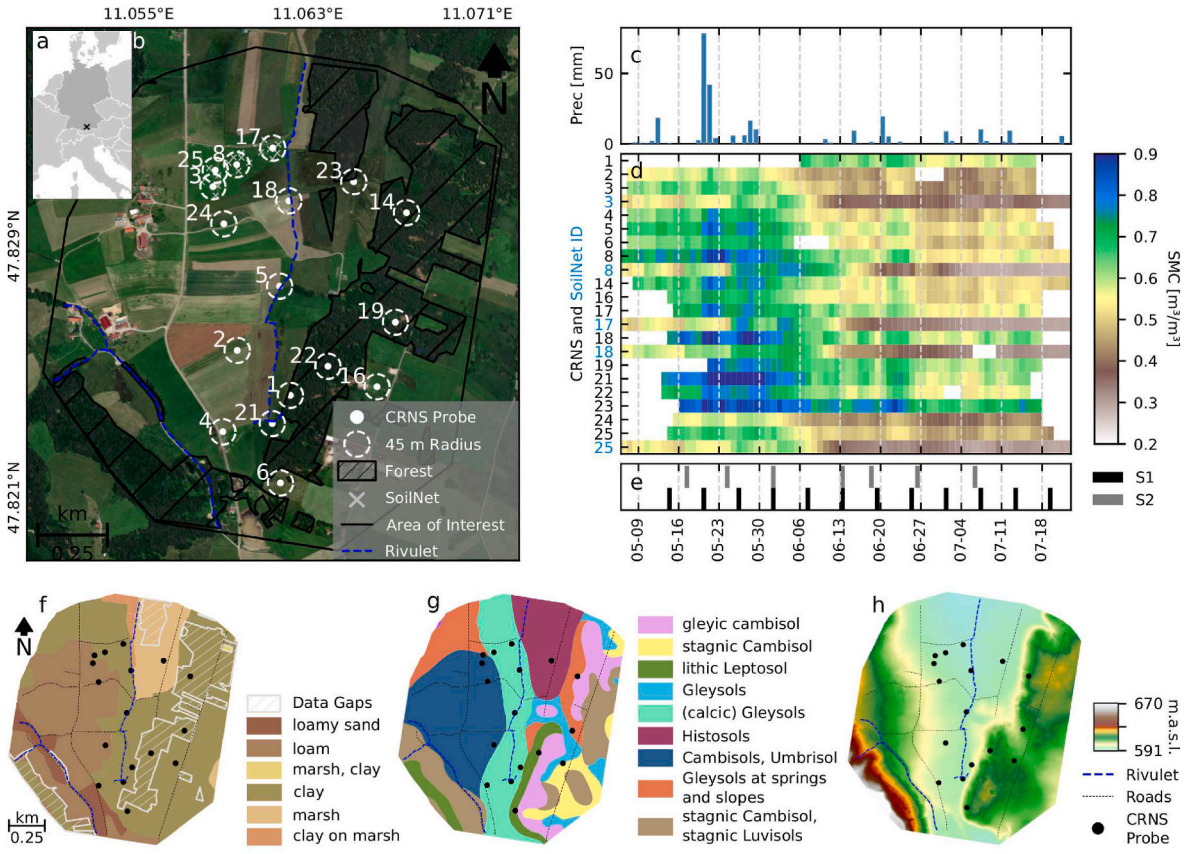

Fig. 1. a) Fendt site within Germany, b) Land cover characteristics of Fendt and CRNS probe locations, c) Precipitation during the observation period, d) SMC data derived by CRNS (black) and SoilNet at 5 cm depth (blue), e) Acquisition dates of the considered remote sensing data (2019), f) Soil texture, g) Soil type, h) Digital elevation model. Base map from ArcGIS World Imagery MapServer. (For interpretation of the references to colour in this figure legend, the reader is referred to the Web version of this article.)

of May, when heavy rainfalls occurred, until approx. June 5, the 5 cm and 20 cm SMC measurements are nearly identical and the CRNS-based SMC signal follows both. During the subsequent dry-down, a bias >0.2 m^3/m^3 evolves between the SMC at 5 cm and 20 cm. Here, the CRNS-based SMC agrees with the SMC at 20 cm depth (Fig. 1 and fig. B.5).

The heavy rainfalls of about 150 mm from May 20–22 and the following inundation and ponding of large areas within the site caused CRNS-based SMC measurements that exceed soil porosity (Heistermann et al., 2021). This is very pronounced for CRNS probe #18, where large offsets between the SoilNet measurements at 5 cm depth and the CRNS estimate exist.

2.3. Satellite and airborne data

We included seven multi-spectral Sentinel 2 (S2) Level 1C scenes acquired from May 5 until July 22 with < 5% cloud cover over the Fendt site (Fig. 1e). We re-sampled the bands with 20 m and 60 m spatial resolution to the spatially higher resolved 10 m bands and calculated spectral indices that are related to SMC, plant vigor or drought stress of plants (see table A.4).

To account for the benefits of a high temporal resolution of SAR systems, we also included twelve Sentinel 1 (S1) Level-1 Ground Range Detected (GRD) data acquired in Interferometric Wide (IW) Swath Mode. The scenes are available in Dual (VV, VH) polarization with a pixel spacing of 10 m × 10 m. We used only ascending scenes, acquired at 17:07 p.m., for better comparability of the different scenes. The acquisition time also ensures that the data is not influenced by dew (Riedel et al., 2002), which occurs at the Fendt site in the morning hours. Post-processing of the GRD-data includes orbit file application, thermal noise removal, GRD-Border-Noise removal, calibration and terrain flattening, speckle filtering and terrain correction. For speckle filtering we applied a 5 × 5 Lee Sigma filter which has been found to be the optimal filter for SMC retrieval in other analyses (Liu et al., 2020). The terrain flattening and correction was based on a LiDAR-based digital elevation Model (DEM) acquired and distributed by the Bayerisches Landesamt für Digitalisierung, Breitband und Vermessung (Landesamt für Digitalisierung, Breitband und Vermessung, 2009) with a spatial resolution of 1 m. Before converting the gamma nought backscatter to decibel, we calculated indices based on VV and VH backscatter values (table A.4). Post-processing was implemented in the Sentinel Application Platform (SNAP) toolbox version 8.0.2.

The LiDAR-based DEM was the basis for the creation of a topographical predictor data set. The DEM was re-sampled to a 10 m spatial resolution to match the lower resolved Sentinel data sets. This data set comprises runoff indicators, wetness indices and a proxy of incoming solar radiation. Table A.4 lists all derivatives of the LiDAR product used in the study.

We averaged all pixels of each data set within a 45 m radius around each CRNS probe. To account for the horizontal footprint characteristics of the CRNS, we applied a revised weighting for averaging as proposed by Schrön et al. (2017). Köhli et al. (2015) state that as a rule of thumb more than half of the CRNS signal originates from the first 50 m around the probe for SMC from 0.0 to 0.5 m^3/m^3. As SMC increases, the radius of main signal contribution declines. With respect to the high SMC at the Fendt site, we consider the 45 m radius to be representative for the sensing range of the CRNS probes. Additionally, a radius of 45 m enables the inclusion of all CRNS probes, but CRNS probe #25, into the Random Forest Regression-model training and testing, because this way the footprints are not overlapping and thus the spatial auto-correlation within the predictor data set is reduced.

2.4. GIS data

To account for the different hydrological processes associated with different soil properties, we included cover fractions of soil type extracted from the Übersichtsbodenkarte of the Bayrisches Landesamt für Umwelt (Bayerisches Landesamt für Umwelt, 2014) as well as soil texture supplied by the Bayrisches Landesamt für Digitalisierung, Breitband und Vermessung within the product Bodenschätzungsdaten (Landesamt für Digitalisierung, Breitband und Vermessung, 2018).

Data gaps of the soil texture product were filled corresponding to the texture descriptions of the soil type product and adjacent soil texture polygons.

Similar to the remote sensing data, we computed weighted coverage fractions by applying the revised weighting after Schrön et al. (2017). Thereby, the weighted cover fraction of a radius r is defined as

$$covFrac = \frac{\sum weights_c}{\sum weights} \quad (1)$$

with the weights being derived as in Schrön et al. (2017) and c being one of the property classes. In the following, we address the GIS and topographical predictor data set as SoilTopo, in conjunction to the remote sensing data sets S1 and S2. The distinction of the predictor set types is based on the temporal variability of the variables and the different remote sensing sensors.

2.5. Random Forest regression

The study aims to gain insight into the coupling of the spatially dynamic CRNS-based SMC signal with remote sensing observations and the corresponding relevance of the different input variables (predictors). Therefore, we opted for the well-known Random Forest regression (RFR) (Breiman, 2001), which balances predictive accuracy and interpretability of results by providing the possibility to infer the individual importance of all incorporated predictors.

To analyze the potential of each data set, we compared different combinations of predictor data types and SMC conditions (Table 1): we implemented a RFR-model for optical (S2) and SAR (S1) only and supplemented both data sets with SoilTopo information (S1SoilTopo, S2SoilTopo). Because of the limited overlap between the acquisition dates of S1 and S2 (Fig. 1e), we did not create a combined model with S1 and S2. Based on the comparison of SoilNet measurements and the CRNS-based SMC signal, we divided the data set into wet and dry periods with June 5th as the cut-off date. By that time, the ongoing dry-down causes a bias > 0.2 m^3/m^3 between SMC measured at 5 cm and 20 cm by the SoilNet. The temporal variability of the CRNS-based SMC within the dry and wet period expressed as mean standard deviation per CRNS probe is listed in Table 1. We modelled SMC for these hydrological conditions with the different sets of predictors (S1_sep, S2_sep, S1SoilTopo_sep, S2SoilTopo_sep). In order to assess the benefit of the temporally varying satellite-borne observations, we created RFR models using only the temporally static SoilTopo data for the respective dates of S2, S2_sep or S1 and S1_sep observations.

Since C-band SAR data is very challenged to estimate SMC under forest and at sites with high natural structures, dominating the backscatter (Jagdhuber, 2012), we removed the affected probes and areas from the analysis of the S1 observations (#1, #14, #19, #21, #22, #23, #25). We also removed data of CRNS probe #2 before June 1 from the analysis (Table 1). The probe is located on the edge of a corn field that was barely covered by vegetation until the first of June, resulting in a very different backscattering signal than for the other samples. For CRNS probe #18 large offsets between near surface SMC and the CRNS-based SMC exist during the wet period, we therefore excluded its measurements until June 5.

To evaluate the different training data, we compared predicted SMC against observations from CRNS by calculating the coefficient of determination (R^2), the root mean square error (RMSE), and the mean absolute error (MAE) by applying a leave-one-out cross-validation (LOO). We extracted the ten most important predictors based on the mean decrease impurity algorithm implemented in the scikit-learn Random

Table 1
Predictor data set, hydrological condition, observed time period, excluded CRNS samples, total number of samples and mean standard deviation per CRNS probe (SD) per RFR-model setup. SoilTopo includes topographical derivatives and soil property information.

model	Hydrological condition	input variables	dates included year: 2019	CRNS probes excluded	nr of samples	SD
S2	mix	S2	05-17 - 07-06	25	122	0.12
S2SoilTopo	mix	S2, SoilTopo	05-17 - 07-06	25	122	0.12
S2_sep						
S2wet	wet	S2	05-17 - 06-01	25, 18	42	0.03
S2dry	dry	S2	06-13 - 07-06	25	78	0.04
S2SoilTopo_sep						
S2SoilTopowet	wet	S2, SoilTopo	05-17 - 06-01	25, 18	42	0.03
S2SoilTopodry	dry	S2, SoilTopo	06-13 - 07-06	25	78	0.04
S1	mix	S1	05-14 - 07-19	25, 23, 14, 19, 22, 1, 21	98	0.11
S1SoilTopo	mix	S1, SoilTopo	05-14 - 07-19	25, 23, 14, 19, 22, 1, 21	98	0.11
S1_sep						
S1wet	wet	S1	05-14 - 06-01	18, 25, 23, 14, 19, 22, 1, 21, 2	29	0.06
S1dry	dry	S1	06-07 - 07-19	25, 23, 14, 19, 22, 1, 21	69	0.04
S1SoilTopo_sep						
S1SoilTopowet	wet	S1, SoilTopo	05-14 - 06-01	18, 25, 23, 14, 19, 22, 1, 21, 2	29	0.06
S1SoilTopodry	dry	S1, SoilTopo	06-07 - 07-19	25, 23, 14, 19, 22, 1, 21	69	0.04

Forest Regression (Pedregosa et al., 2011). For S2 RFR-models, forest areas are included. Enabling a comparison of the results with S1 RFR-models, we analyzed the RFR-model metrics for grassland and forest areas separately. Using the best S1 and S2 RFR-models, we applied the relationship to the whole Fendt site for a day of high and low SMC. We compared the results to a constrained interpolation of the CRNS-based SMC as published recently by Heistermann et al. (2021).

3. Results

The Fendt site characteristics and the dense network of CRNS probes is beneficial for analyzing the linkage of S1 and S2 observations as well as SoilTopo variables with CRNS-based SMC. The fact that the CRNS-based SMC data set comprises high spatio-temporal gradients with SMC ranging from 0.2 m^3/m^3 to 0.9 m^3/m^3 enables the analysis of the impact of dry and wet periods on this relationship.

3.1. Following the CRNS-based SMC with Sentinel 2 observations

In Fig. 2 we display the RFR-model fit and their ten most important predictors. Table 3 details the corresponding statistical metrics and the RFR-model performances of the associated SoilTopo_only models (see also fig. C.6). When only S2 data are used as RFR-model input, we see a modest ability to predict SMC with an R^2 of 0.45, accompanied by severely under- and over-estimated samples. The S2SoilTopo RFR-model

Table 2
Model performance of S1_sep and S2_sep for forest and grassland areas.

hydrological condition	S1_sep		S2_sep grass		S2_sep forest	
	RMSE	R^2	RMSE	R^2	RMSE	R^2
wet	0.08	0.34	0.11	0.13	0.07	0.30
dry	0.1	0.03	0.07	0.21	0.06	0.46

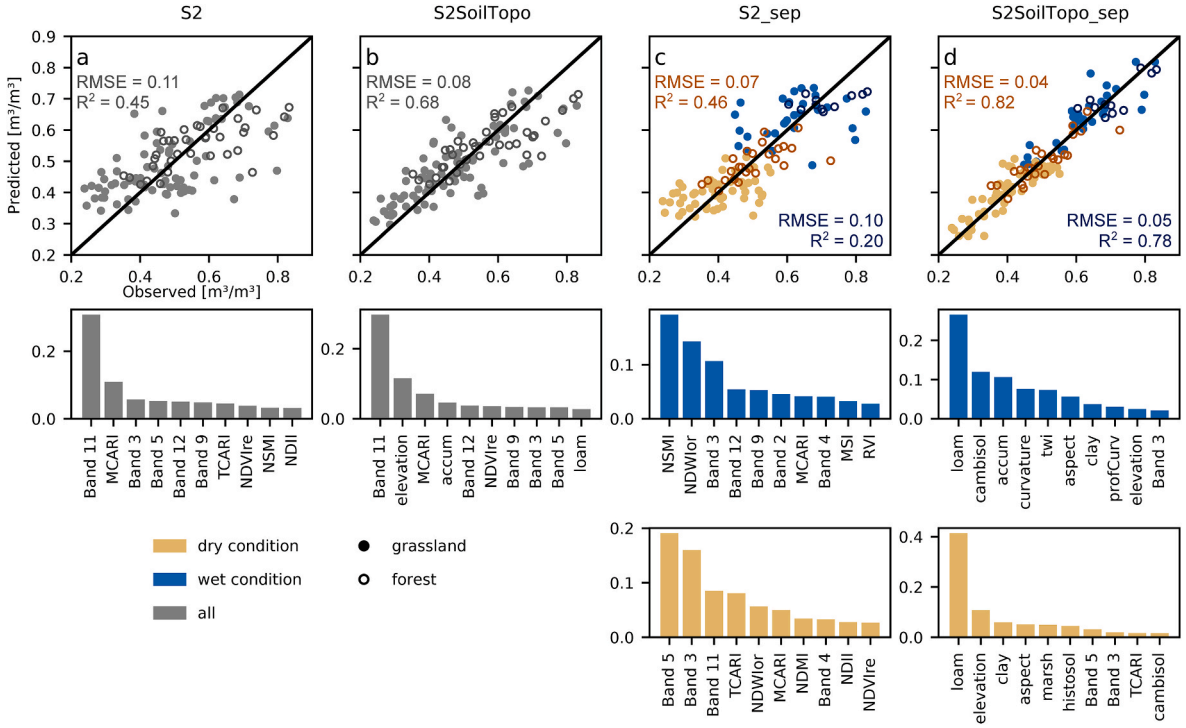

Fig. 2. Observed and LOO-Predicted SMC and the 10 most important predictors of the RFR-model a) Sentinel 2 data alone (S2) b) Sentinel 2 and soil type and topography data (S2SoilTopo) c) Sentinel 2 for the dry and wet period (S2_sep) d) Sentinel 2 and SoilTopo data for the dry and wet period (S2SoilTopo_sep).

Table 3
Model performance of the different Random Forest regression model setups.

Model name	RMSE		MAE		R^2	
	Model	SoilTopo_only	Model	SoilTopo_only	Model	SoilTopo_only
S2	0.11	0.13	0.09	0.12	0.45	0.21
S2SoilTopo	0.08	0.13	0.06	0.12	0.68	0.21
S2_sep						
S2wet	0.10	0.04	0.08	0.03	0.20	0.85
S2dry	0.07	0.05	0.06	0.04	0.46	0.78
S2SoilTopo_sep						
S2SoilTopowet	0.05	0.04	0.04	0.03	0.78	0.85
S2SoilTopodry	0.04	0.05	0.03	0.04	0.82	0.78
S1	0.14	0.13	0.11	0.11	0.07	0.16
S1SoilTopo	0.12	0.13	0.09	0.11	0.26	0.16
S1_sep						
S1wet	0.08	0.08	0.06	0.06	0.34	0.37
S1dry	0.10	0.04	0.08	0.03	0.03	0.76
S1SoilTopo_sep						
S1SoilTopowet	0.06	0.08	0.05	0.06	0.61	0.37
S1SoilTopodry	0.04	0.04	0.03	0.03	0.76	0.76

and also – to a lesser extent – the S2 RFR-model are able to separate wet (May 17 to June 1) from dry (June 13 to July 6) periods. For both RFR-models, Band 11, located in the short wave infrared wavelength range (1610 nm), is the most skillful predictor.

During the dry period, the mean observed SMC under forest is 0.1 m^3/m^3 higher than the SMC under grassland areas. All established S2-based RFR-models reproduce this land cover-specific SMC difference.

Modelling wet and dry periods separately (S2_sep) improves the overall RFR-model performance of S2. However, the performance between grassland and forest areas differs distinctively for the S2_sep model (Fig. 2c). The RFR-model metrics of S2_sep distinguished by land cover type are displayed in Table 2. Grassland with a maximum R^2 of 0.21 shows no correlation to SMC, whereas forest areas show moderate R^2 of 0.3 and 0.46 for the wet and dry model, respectively.

SoilTopo as additional predictor set is considerably reducing the RMSE of S2 and S2_sep wet and dry RFR-models up to 50%. This is underlined by the most important variables of the RFR. Within the S2SoilTopowet model, six out of ten predictors are topography derivatives that account for flow properties. For the S2SoilTopodry RFR-model, in turn, half of the ten most important predictors are based on soil property information. S2 observations only play a minor role within both S2SoilTopo_sep RFR-models. This is revealed by only one and three S2 based indicators for wet and dry periods, respectively.

Using the SoilTopo_only models as a benchmark (Table 3, see also fig. C.6), it becomes apparent that S2 data provide valuable temporal information to the S2, S2SoilTopo, and S2SoilTopodry RFR-models. This is also confirmed by the scatterplot Fig. 2d, where no distinct horizontal lines are visible. The S2SoilTopowet model has lowest temporal variability with an averaged standard deviation of 0.3 per CRNS probe. For this RFR-model, using only SoilTopo variables to predict the CRNS-based SMC is more accurate than adding S2 observations.

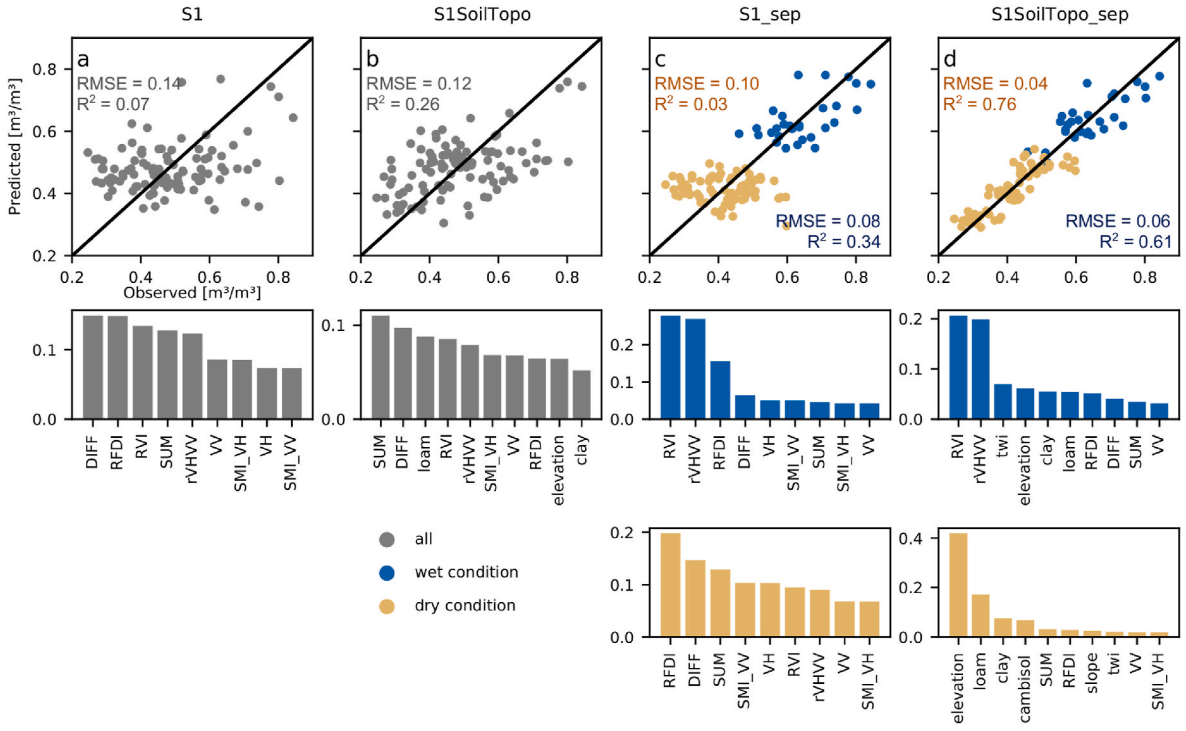

Fig. 3. Observed and Predicted SMC and 10 most important input variables of the RFR-model a) Sentinel 1 data alone b) Sentinel 1 and SoilTopo information c) Sentinel 1 separated by wet and dry period d) Sentinel 1 and SoilTopo information separated by wet and dry period.

3.2. Following the CRNS-based SMC with Sentinel 1 observations

The results of the S1 regression, as depicted in Fig. 3, reveal a low RFR-model performance when not accounting for soil wetness conditions. When modelling dry and wet periods separately, only the RFR-model of the wet period reaches a modest performance with an R^2 of 0.34 and an RMSE of 0.17 m^3/m^3.

Including soil and topography information to the predictors reduces the RSME of the S1dry and S1wet RFR-models by 60% and 25%, respectively. Similar to the S2SoilTopo_sep RFR-models, the majority of the most important variables in the S1SoilTopodry RFR-model are SoilTopo variables. Particularly relevant for the S1SoilTopodry RFR-model is the information about the soil properties. The wet RFR-model in turn is rather based on topographical derivatives. Besides SoilTopo predictors, also the radar vegetation index (RVI) and the ratio VH/VV (rVHVV) are very relevant for the S1 RFR-models with modest to good RFR-model performance (S1wet and S1SoilTopowet RFR-models).

S1 observations do not improve the S1SoilTopodry RFR-model. As with the S2SoilTopowet model, temporal variability is lowest for the S1SoilTopowet RFR-model with a mean standard deviation per CRNS probe of 0.04 m^3/m^3. In contrast, for the more temporally variable (0.06 m^3/m^3) wet period, the S1 observations add necessary temporal information. This is reflected in a 25% lower RMSE and a nearly doubled R^2 of the S1SoilTopowet RFR-model compared to the corresponding SoilTopo_only RFR-model.

3.3. Spatial application of Random Forest Regression models

The spatial application of the best RFR-models in comparison to a constrained interpolation of the CRNS-based SMC is depicted in Fig. 4 for June 1 for all RFR-models and June 25 and June 26 for S1-based and S2-based RFR-models, respectively. Each pixel value of the RFR-model predictions corresponds to a CRNS-based SMC signal that is an integrated SMC estimate of a footprint with horizontal scale larger then the pixel itself. Moreover, the vertical extent of the soil medium which contributes to the SMC signal varies for each pixel due to different soil properties, SMC and different hydrogen pools (Baroni et al., 2018; Köhli et al., 2015, 2021).

All RFR-models are able to differentiate between the wetter mean SMC of 0.64 m^3/m^3 of June 1 and the drier mean SMC of 0.43 m^3/m^3 of June 26. However, the spatial distributions of the predictions differ significantly. The constrained interpolation (a) depicts areas of SMC higher than 0.75 m^3/m^3 in the northern part of the Fendt site for the wet day. These are also captured by the two S2-based RFR-models (c, d), but the high SMC values are limited to the course of the rivulet. The drier western area of the Fendt site is reproduced by all applied RFR models. However, the spatial heterogeneity in SMC is less pronounced for the S1SoilTopo_sep (b, f) compared to the S2-based RFR-models. For the S1SoilTopodry RFR-model (f) as well as the S2SoilTopowet (c) and S2SoilTopodry (g) RFR-models, the spatial distribution of soil properties shapes the predicted SMC pattern. Within these prevailing patches, the RFR-model still differentiates between wetter and drier areas. In contrast, the spatial distribution of SMC estimated by S2SoilTopo (d, h) strongly follows field structures and grass mowing patterns. Similar patterns are revealed within the S1SoilTopowet RFR-model (b).

4. Discussion

Our goal was to provide initial insights into the potential of S2 and S1 as well as ground and topography information in following the SMC of a large soil volume as obtained by CRNS. In this regard, we applied RFR trained with different predictor combinations and for different soil wetness conditions.

In general, our analysis showed that both sensors, S1 and S2, could be linked to CRNS-based SMC data for certain time periods and to a certain spatial extent. We will address the space-borne observation related results in section 4.1 and section 4.2. Our results also showed the high importance of soil and topography information in estimating the CRNS-based SMC, which will be discussed in section 4.3. In section 4.4 we evaluate the limitations and possibilities of the developed approach.

4.1. Following CRNS-based SMC with Sentinel 2 observations

The model performances of S2-based RFR-models that do not account for wet and dry periods, show the ability of S2 observations to distinguish between wet and dry CRNS-based SMC. The S2 and S2SoilTopo RFR-models are mainly driven by SWIR bands, especially band 11, and spectral indices that include bands of the SWIR, such as the normalized difference infrared index (NDII) or the normalized soil moisture index (NSMI). These results confirm the high potential of the SWIR bands to distinguish moisture states of soil and plant material (Ambrosone et al., 2020; Sadeghi et al., 2017; Shih and Jordan, 1992).

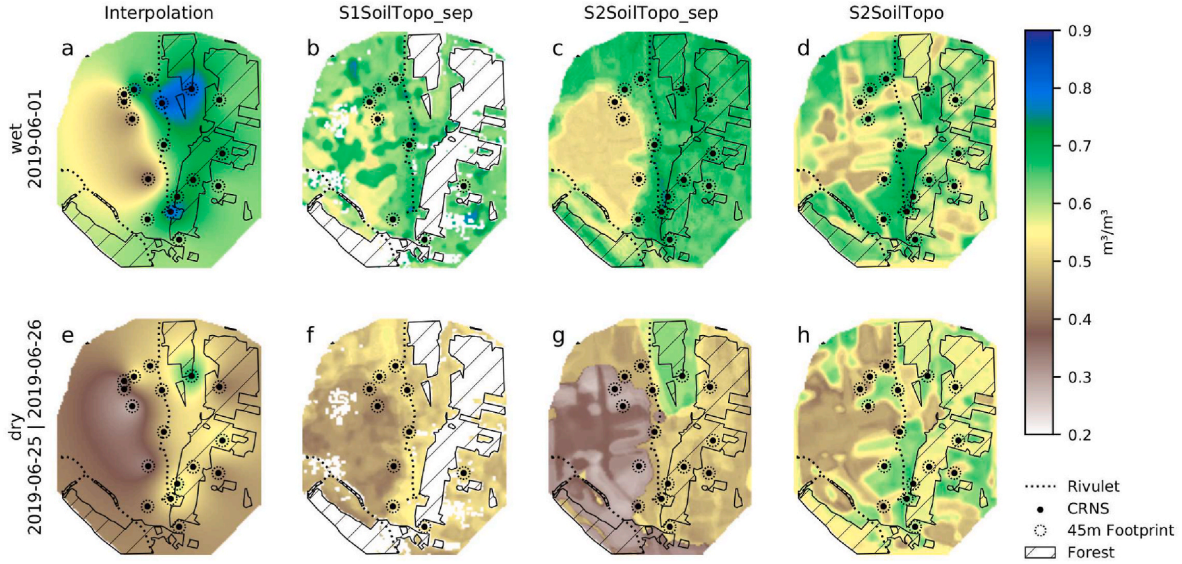

Fig. 4. **a,e** Constrained Interpolation of CRNS-SMC and spatial application of **b,f** S1SoilTopo_sep **c,g** S2SoilTopo_sep **d,h** S2SoilTopo for **a,b,c,d** July 1, **f** June 25 and **e,g,h** June 26. Black dots mark CRNS probes included for the corresponding model training.

The S2 and S2SoilTopo models, which do not distinguish between wet and dry periods, imply that S2 is not affected by the decreasing penetration depth of the CRNS-based SMC signal with wetter soils. Plant characteristics, similar to the CRNS-based SMC signal, are indicators of SMC at depths that change with hydrologic condition (Fort et al., 2017; Guderle et al., 2018; Hildebrandt, 2020; Nippert and Knapp, 2007). Best correlations between SMC and spectral indices can be obtained for the SMC at the depth of maximum root water uptake (Carlson et al., 1990; Peng et al., 2014; West et al., 2018). Nippert and Knapp (2007) and Guderle et al. (2018) find depths of maximum water uptake of grassland species ranging from 5 cm at saturated conditions to 60 cm during dryer periods. This approximates the vertical characteristics of the CRNS-based SMC signal in our analysis. The SMC of the CRNS corresponds best with the SMC measured by SoilNet at 5 cm and 20 cm depth during wet and dry periods, respectively.

S2 models are also able to map the land cover specific SMC distribution with grassland having a lower SMC than forest areas during the dry period. A multitude of analyses found that SMC distribution and dynamics differ with land cover type (Korres et al., 2010; Vinnikov et al., 1996; Wang et al., 08 2012). Optical data has shown to be able to map the land cover specific SMC using a variety of approaches (Ambrosone et al., 2020; Liu et al., 2020; Sadeghi et al., 2017; Sobrino et al., 2012). Since S2 data are highly suitable for land cover mapping (Ottosen et al., 2020; Rujoiu-Mare et al., 2017; Sánchez-Espinosa and Schröder, 2019), the successful discrimination of land cover specific SMC in our results can be expected for the small forest-grassland area considered in this study.

The poor grassland specific RFR-model performances of S2_sep and the spatial prediction of S2SoilTopo reveal the disadvantage of relying only on vegetation traits. The Fendt site encompasses large areas of intensively managed grassland. The small-scale cutting practices combined with pastures result in a patchwork of diverse regrowth stages within the study area which hampers the linkage of CRNS-based SMC with S2 data. Burke et al. (1998) found that mowing is able to override the dependency of vegetation traits on SMC.

Consistent with the mowing activities that hamper SMC-retrieval at the grassland areas, for the non-managed forest sites the wet and dry RFR-models are able to follow the CRNS-based SMC. Since significant soil depth and species dependent time lags of optimal vegetation response exist (Naithani et al., 2013; Peng et al., 2014), this correlation could be further enhanced with a time lag analysis for the Fendt site.

4.2. Following the CRNS-based SMC with Sentinel 1 observations

For S1 data it is crucial to distinguish between dry and wet periods, thus accounting for the different sensing volumes of S1 observations and CRNS. Our results of the S1 and S1SoilTopo RFR-models reveal difficulties to follow the CRNS-based SMC despite the successful surface SMC retrievals with S1 data reported at grassland (Holtgrave et al., 2018) and farmland sites (El Hajj et al., 2017; Liu et al., 2020). The superior RFR-model fit of the wet over the dry RFR-model of S1_sep shows the impact of the different vertical extent of the two sensing techniques. The SMC obtained by CRNS during the wet period corresponds to the SMC measured at 5 cm depth by the SoilNet. The penetration depth of the C-band waves reaches a maximum of 10 cm for bare soil (Ulaby et al., 2014). Owe and Van de Griend (1998) find an effective penetration depth of 1–2 cm. The similar sensing sensitivity of the C-Band microwave and the CRNS to similar soil volumes during the wet period lead to the successful linkage of both signals. Due to the deepening of the vertical sensing extent of the CRNS with decreasing SMC (Köhli et al., 2015; Schrön et al., 2017), the bias between SMC obtained by CRNS and the SMC of the shallower sensing volume of the S1 increases during the dry hydrological period. This results in poorer correspondence of CRNS-based SMC with S1 during this period.

Wet RFR-models of S1_sep and S1SoilTopo_sep are impacted by vegetation cover. This is visible in the spatial application of the S1SoilTopowet RFR-model, and the importance of the ratio of VV and VH (rVVVH) and the Radar vegetation index (RVI) for the RFR-model creation. Comparisons of the SAR indices with plant traits and spectral indices (Holtgrave et al., 2020; Veloso et al., 2017) found good agreement with NDVI and NDWI time series as well as biomass and and green area index for different crops. This indicates that the RFR-model uses the sensitivity of the microwave to the water conditions and dynamics in the vegetation, which in turn are based on soil water dynamics (Porporato et al., 2001). But, similar to the S2SoilTopo RFR-model, the spatial patterns of the S1SoilTopowet RFR-model follow the field structures. This demonstrates that also for SAR the indicative value of plant characteristics for soil moisture is disturbed by mowing, as it leads to an inconsistent signal attenuation by the varying vegetation cover along space and time.

SoilTopo as additional data set is essential to support S1-based RFR-models. Directly affecting S1 data, the dielectric constant varies with soil texture. Engman and Chauhan (1995) rate this impact of the soil texture on the dielectric constant as less relevant for practical purposes. Contrasting this, Beale et al. (2019) report errors of up to 20 vol_% when the spatial distribution of soil properties such as texture, organic matter content and structure are not considered in the SMC retrieval at resolutions <100 m. Accounting for soil texture was especially beneficial for the S1SoilTopodry RFR-model.

4.3. Contribution of soil properties and topography information

All RFR-models considerably benefit from the inclusion of soil and topography information in the predictor data set. Especially in S1SoilTopo_sep and S2SoilTopo_sep, variables of SoilTopo are the most important predictors in estimating SMC. This is in accordance to analyses on the driving factors of SMC patterns in different watersheds that identify topography and soil properties as the most important features (Korres et al., 2010; Rosenbaum et al., 2012).

A major drawback of the SoilTopo data set is its temporally static character. Obviously, this inhibits RFR-models with only SoilTopo as input to estimate temporal variability. Splitting the CRNS data into wet and dry periods allows the selection of those SoilTopo predictors that best represent the patterns of SMC during each hydrological period. Also Western et al. (1998) and Schröter et al. (2015) find better model capacity of topographic SMC modelling when taking soil wetting and drying phases into account, since the explaining capacity of the different predictors varies with SMC condition and governing physical processes.

In the dry RFR-model of both, S1SoilTopo_sep and S2SoilTopo_sep, soil texture and soil type information are the most important predictors, followed by elevation. For the wet RFR-models, topography derivatives related to runoff are the major contributors. This is in accordance to other investigations on SMC patterns. They find that lateral flow and redistribution processes dominate the SMC patterns during wet periods (Grayson et al., 1997; Rosenbaum et al., 2012; Western et al., 1998). Soil properties controlling water holding capacity (Vereecken et al., 2007) and topographical information related to solar energy driving evapotranspiration (Western et al., 1998) in turn are drivers of SMC distribution during dry states. If the temporal variability within the hydrological states is too high, additional information of the space-borne sensors are necessary to add the temporal dynamics prevalent within the SMC clusters.

4.4. Limitations and potentials

A variety of analyses underline the potential of the synergistic use of S2 and S1 in retrieving SMC (Attarzadeh et al., 2018; Liu et al., 2020; Paloscia et al., 2013). However, no combined RFR-model with both, S1 and S2, as predictors was established in this study. During the here considered observation time, only five image acquisitions of S1 and S2 have a maximum time difference of one day. With longer time intervals between data acquisitions, alterations of the land surface due to mowing

activities occur. Four of the five overlapping S1 and S2 acquisition dates are within the dry period, during which the different sensing volumes of S1 and CRNS limit the explanatory power of the RFR-model. Extending the predictor set by SoilTopo leads to higher model performance, but S1 and S2 data are the less important predictors. Therefore, with the data set used here, it is not expected that a combination of S1 and S2 will lead to new insights into the relation of the CRNS-based SMC and the remote sensing signals.

Both remote sensing observations were weighted corresponding to Schrön et al. (2017) within a radius of 45 m for each CRNS probe. The overall footprint extent of the CRNS probe actually exceeds the here chosen radius (Köhli et al., 2015). However, the majority of the CRNS signal originates from the first 50 m around the CRNS probes. With increasing soil wetness, the area of major signal contribution recedes even closer to the probe (Köhli et al., 2015). Thus, we assume that the chosen footprint extent is representative to draw our conclusions. However, the impact of the weighting method and the horizontal extent chosen to determine the footprint in the S1 and S2 observations requires further analysis.

We are now better understanding the potentials and limitations of S1, S2 and SoilTopo data in following the CRNS-based SMC signal. However, the insights are confined to C-band SAR data characteristics, the S2 specific optical observations, the site characteristics of the Fendt area (grassland only) and the observed season (spring - summer). So far, we only analyzed the linkage of VV- and VH-polarized C-Band observations with the CRNS-based SMC signal. The HH polarization (Paloscia et al., 2013) or the deeper penetrating L- and P-Band microwaves may be better related to SMC and differ in sensing volume (El Hajj et al., 2019; Ulaby et al., 2014). This is of special interest since the recently launched SAOCAM and other upcoming L-Band satellite missions such as NISAR, ROSE-L and Tandem-L will deliver high resolution SAR data at very high temporal resolutions. Not only S2 and S1 observations (Esch, 2018; Mengen et al., 2021; Schnur et al., 2010) but also the dynamics of CRNS-based SMC signal (Baroni et al., 2018; Köhli et al., 2021) are species, soil and land cover dependent (Esch, 2018; Mengen et al., 2021; Schnur et al., 2010). Therefore, further analyses are needed at other sites with different land cover characteristics to confirm our first findings.

According to our results, there are optimal hydrological conditions especially for S1 but also for variables of SoilTopo to follow the CRNS-based soil moisture. In this analysis we split the data into dry and wet periods based on in-situ (SoilNet) information existing at the Fendt site. Such temporal continuous and extensive reference SMC measurements are not available at all sites. Finding a method or a data set to stratify the CRNS-based SMC signal corresponding to hydrological conditions such as precipitation history, large scale SMC products of satellite missions or hydrological simulation models are welcome options to apply the approach at other sites and beyond the reported study setup.

One of the advantages of satellite remote sensing is the ability to extend and complement local ground-based measurements for a larger region. This analysis is a local experiment to identify and understand the potentials and impacts when linking remote sensing observations with CRNS-based SMC. However, for transferring data-driven models to other sites their training samples need to comprise the whole range of SMC, vegetation, soil properties and climate conditions (Schnur et al., 2010). Mobile versions of CRNS, such as roving or the application of CRNS on trains (Desilets et al., 2010; Schrön et al., 2021) provide CRNS-based SMC over a broad range of environmental characteristics. As such, it is a promising data source for developing a novel SMC product at the regional level.

Using large scale CRNS-based SMC as reference data for mapping SMC is beneficial due to several reasons: CRNS-based SMC has been shown to be superior over point measurements in representing hydrological processes at the catchment scale (Dimitrova-Petrova et al., 2020). Additionally, the horizontal footprint of the CRNS method may correspond to the spatial extent of space-borne remote sensing observations (Mohanty et al., 2017) and provides SMC estimates at the so far poorly represented intermediate scale (Robinson et al., 2008). One of the major benefits of the CRNS method is its sensing depth up to 80 cm (Köhli et al., 2015) thus representing the poorly represented (Peng et al., 2021) root zone SMC especially during the critical dry periods. Using Random Forest regression models and evaluating the potentials of S1 and S2, we have shown for the first time that it is possible to follow the larger sensing volume of the CRNS in space and time using multi-source remote sensing observations at a well known site. In doing so, we showed the possibility to exploit the favourable large vertical penetration depth of the CRNS method.

5. Conclusion

This analysis set out to provide insights into the machine learning-based linkage of SMC signals that vary in space and time, namely optical (S2) and active microwave (S1) remote sensing observations, time-invariant site specific information (soil type and topography) and the space-time dynamic CRNS-based SMC. It was built on an unique experimental data set of CRNS-based SMC that encompasses strong spatial and temporal SMC dynamics of an entire sub-catchment including ponding situations and a subsequent dry-down at different land cover types, soil properties, and topographic settings.

By using different Random Forest regressions (RFR) to follow CRNS-based SMC with S2, S1 as well as site specific data, we identified sensor specific spatio-temporal conditions that influence this data-driven linkage.

Based on in-situ SoilNet measurements, we defined a wet and dry period. During the wet period, the CRNS-based SMC corresponds to the SMC at 5 cm depth, whereas for the dry period the CRNS-based SMC follows measurements taken at depths of 20 cm. The RFR-models based on optical S2 data are able to differentiate between very wet and dry periods. The retrieval of CRNS-based SMC with S2 observations is less affected by the spatial dynamics of the CRNS-based SMC signal with hydrological condition as it is sensitive to plant rather than soil properties. The dependency on plant traits also allows S2 data to distinguish land-cover-specific SMC differences for grassland and forest. However, grass mowing practices of the farmers hamper the retrieval of SMC patterns for S2 data within the grassland land cover class. For the quasi-unmanaged forest sites, it was possible to follow the CRNS-based SMC signal with S2-based RFR-models. These RFR-models require additional information of topography and soil texture in order to account for their impact on water availability for plants.

For linking S1 with CRNS-based SMC, it is crucial to consider wet and dry periods. RFR-modelling with S1 data was only successful for the wet period when the CRNS-based SMC signal corresponded to the top-soil (5 cm) SMC. Similar to S2-based RFR-models, S1-based RFR-models are impacted by grass mowing practices due to inconsistent signal attenuation along the vegetation canopy. Also the individual S1-based RFR models for wet and dry periods are improved by soil texture and topography information.

Accounting for the hydrological conditions enables the RFR-models to select variables from the soil property and topography data set that are indicative for the corresponding hydrological processes during wet and dry periods. For the dry period, soil properties and topography variables relating to solar energy input are the most important information for estimating CRNS-based SMC. For the wet period, the topographic indicators of runoff distribution contribute most to the regression model. Whilst the information on soil and topography represent a general time-static pattern of SMC distribution for each hydrological condition, the S1 and S2 data add the temporal dynamics to these clusters. Taken together, these results underline the importance to make use of the advantages of all data sources.

This study shows the potential of exploiting the large sensing volume of the CRNS method via a data-driven linkage with remote sensing observations. It provides first insights into the synergy of different spatio-temporal data sets when following the space-time-dynamic SMC signal

of CRNS. Understanding the potentials and limitations of each sensor is relevant when targeting the combined use of different data sources in space and time for a better coverage and understanding of hydrological processes in the vadose zone at larger spatial scales.

Funding

This work was supported by the Deutsche Forschungsgemeinschaft (DFG, German Research Foundation) (project 357874777 of the research unit FOR 2694 "Cosmic Sense", 2018). The Terrestrial Environmental Observatory (TERENO) Pre-Alpine infrastructure is supported by the Helmholtz Association and the Federal Ministry of Education and Research.

Author's responsibilities

V.D. and M.F. conceived of the research idea; T.F. and M.H. processed the CRNS data; V.D. performed statistical analyses; V.D., with contributions from T.J. and M.F., wrote the paper; all authors discussed the results and commented on the manuscript.

Declaration of interests

The authors declare that they have no known competing financial interests or personal relationships that could have appeared to influence the work reported in this paper.

Acknowledgments

Base map data contributed by: Esri, Maxar, GeoEye, Earthstar Geographics, CNES/Airbus DS, USDA, USGS, AeroGRID, IGN, and the GIS User Community. We want to thank Florencia Arias for contributing to the selection of the Sentinel 1 and Sentinel 2 observations.

Appendix A. Predictor Variables

Table A.4
Optical and SAR indices as well as topographical derivates included in the predictor data sets

Name	Formula or algorithm	Parameter	Ref.
Optical indices			
NDVI	$(NIR - B4)/(NIR + B4)$		Rouse et al. (1974)
NDVI_sc	$(NDVI - NDVI_{bS})/(NDVI_{vC100} - NDVI_{bS})$	bS: bare Soil, vC100: veg Cover 100%	Sobrino et al. (2012)
EVI	$G \times (NIR - B4)/(NIR + C1 \cdot B4 - C2 \cdot B2 + L)$	$G = 2.5, C1 = 7.5, L = 1$	Huete et al. (1996)
$NDVI_{705}$	$(B6 - B5)/(B6 + B5)$		Sims and Gamon (2002)
RVI	$B8/B4$		Pearson and Miller (1972)
MCARI	$(B5 - B4) - 0.2(B5 - B3)(B5/B4)$		Daughtry et al. (2000)
TCARI	$3[(B5 - B4 - 0.2(B5 - B3)(B5/B4)]$		Haboudane et al. (2002)
MSAVI	$0.5(2 \cdot B8 + 1 - [(2 \cdot B8 + 1)^2 - 8(B8 - B4)]^{0.5})$		Qi et al. (1994)
NSMI	$(B11 - B12)/(B11 + B12)$		Haubrock et al. (2008)
SAVI	$[(B8A - B4)(1 + L)]/(B8A + B4 + L)$	L: 0.5	Huete (1988)
NDWIor	$(B3 - B8)/(B3 + B8)$		McFeeters (1996)
NDII	$(B8 - B11)/(B8 + B11)$		Hardisky et al. (1983)
MSI	$(B12)/(B8)$		Rock et al. (1986)
NDMI	$[B8A - (B11 - B12)]/[R_{860nm} + (B11 - B12)])$		Wang and Qu (2007)
SAR indices			
rVHVV	VV/VH	γ^0	Veloso et al. (2017)
RVI	$4VH/(VH + VV)$	γ^0	Nasirzadehdizaji et al. (2019)
RFDI	$(VV - VH)/(VV + VH)$	γ^0	Saatchi (2019)
SUM	$VV + VH$	γ^0	
DIFF	$VV - VH$	γ^0	
SMI_VV	$(VV - VV_{min})/(VV_{max} + VV_{min})$	γ^0	Esch (2018)
SMI_VH	$(VH - VH_{min})/(VH_{max} + VH_{min})$	γ^0	after Esch (2018)
Topographical derivates			
elevation		masl	
slope	Barnes (2016)	radians	Horn (1981)
aspect	Barnes (2016)	degree	Horn (1981)
curvature	Barnes (2016)		Zevenbergen and Thorne (1987)
profile curvature	Barnes (2016)		Zevenbergen and Thorne (1987)
planform curvature	Barnes (2016)		Zevenbergen and Thorne (1987)
Flow accumulation	Rho8 implemented in Barnes (2016)		Fairfield and Leymarie (1991)
TWI	$ln(FlowAccum/tan(slope))$	Flow accumulation, slope	BEVEN and KIRKBY (1979)

Appendix B. . SoilNet soil moisture vs. CRNS soil moisture

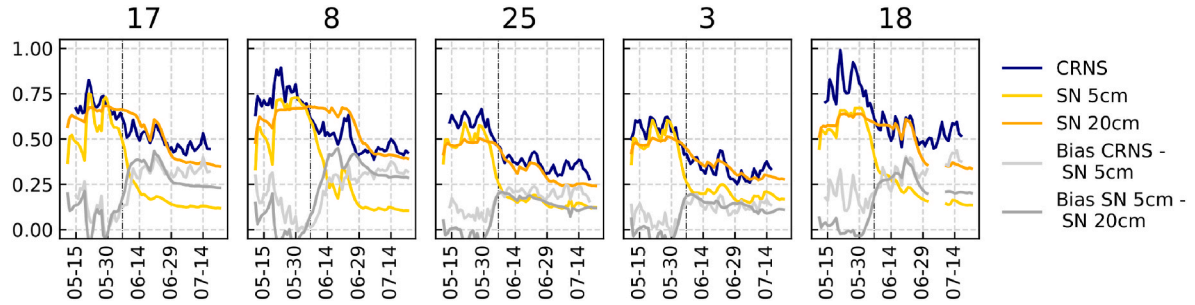

Fig. B.5. Comparison of averaged SMC derived from SoilNet Nodes within a 60 m radius to the individual CRNS probes at 5 cm and 20 cm depths with the CRNS-based SMC. The dashed black line marks the cut-off date between the wet and dry periods.

Appendix C. . SoilTopo_only RFR models for S1 and S2 acquisition dates

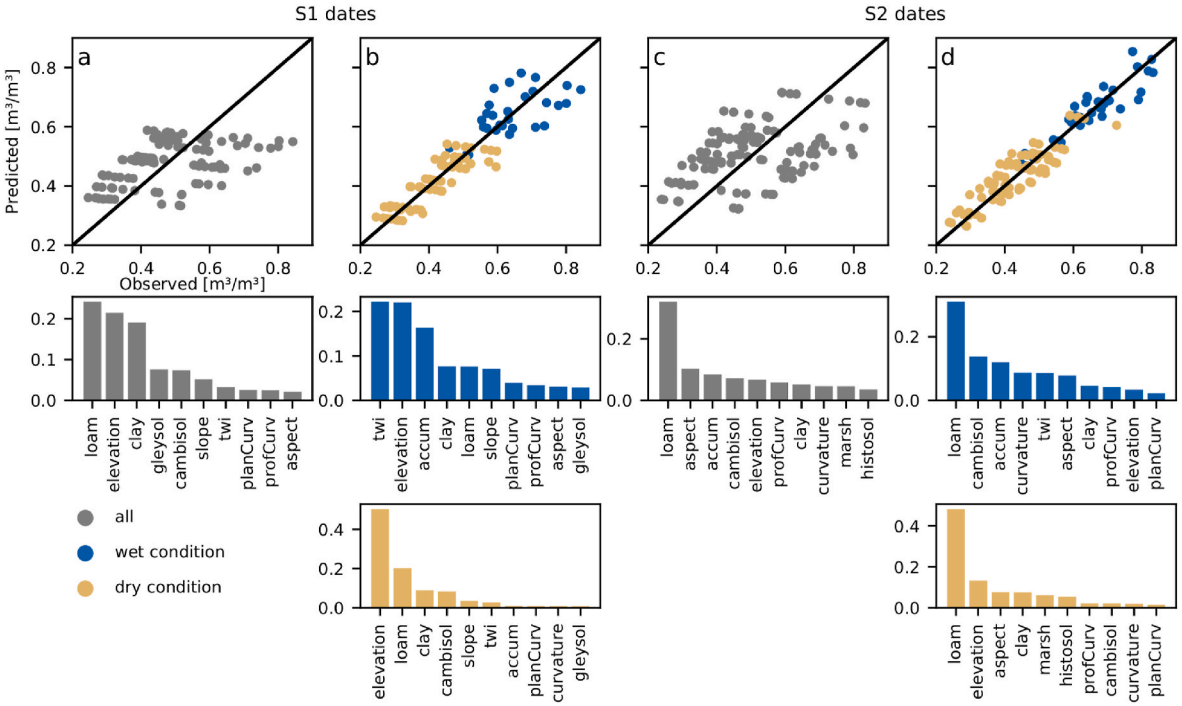

Fig. C.6. Observed vs. Predicted CRNS-based SMC using only SoilTopo data a) SoilTopo_only for S1 dates b) SoilTopo_only for S1 acquisition dates separated by hydrological condition c) SoilTopo_only for S2 acquisition dates d) SoilTopo_only for S2 acquisition dates separated by hydrological condition.

References

Ambrosone, M., Matese, A., Di Gennaro, S.F., Gioli, B., Tudoroiu, M., Genesio, L., Miglietta, F., Baronti, S., Maienza, A., Ungaro, F., Toscano, P., 2020. Retrieving soil moisture in rainfed and irrigated fields using sentinel-2 observations and a modified optram approach. Int. J. Appl. Earth Obs. Geoinf. 89, 102113.

Andreasen, M., Jensen, K.H., Desilets, D., Franz, T.E., Zreda, M., Bogena, H.R., Looms, M. C., 8 2017. Status and perspectives on the cosmic-ray neutron method for soil moisture estimation and other environmental science applications. Vadose Zone J. 16 (8), 1–11.

Attarzadeh, R., Amini, J., Notarnicola, C., Greifeneder, F., 2018. Synergetic use of sentinel-1 and sentinel-2 data for soil moisture mapping at plot scale. Rem. Sens. 10 (8), 1285.

Baatz, R., Bogena, H.R., Hendricks Franssen, H.-J., Huisman, J.A., Montzka, C., Vereecken, H., 2015. An empirical vegetation correction for soil water content quantification using cosmic ray probes. Water Resour. Res. 51 (4), 2030–2046. URL. https://agupubs.onlinelibrary.wiley.com/doi/abs/10.1002/2014WR016443.

Bablet, A., Vu, P.V.H., Jacquemoud, S., Viallefont-Robinet, F., Fabre, S., Briottet, X., Sadeghi, M., Whiting, M.L., Baret, F., Tian, J., 2018. MARMIT: a multilayer radiative transfer model of soil reflectance to estimate surface soil moisture content in the solar domain (400–2500 nm). Remote Sens. Environ. 217, 1–17. URL. https://www.sciencedirect.com/science/article/pii/S0034425718303651.

Baghdadi, N., El Hajj, M., Zribi, M., Bousbih, S., 2017. Calibration of the water cloud model at c-band for winter crop fields and grasslands. Rem. Sens. 9 (9), 969.

Barbosa, L.R., Coelho, V.H.R., Scheiffele, L.M., Baroni, G., Ramos Filho, G.M., Montenegro, S.M.G.L., Almeida, C.d.N., Oswald, S.E., 2021. Dynamic groundwater recharge simulations based on cosmic-ray neutron sensing in a tropical wet experimental basin. Vadose Zone J. 20 (4), e20145. _eprint: https://acsess.onlinelibrary.wiley.com/doi/pdf/10.1002/vzj2.20145 https://acsess.onlinelibrary.wiley.com/doi/abs/10.1002/vzj2.20145.

Barnes, R., 2016. RichDEM: terrain analysis software. URL. http://github.com/r-barnes/richdem.

Baroni, G., Scheiffele, L., Schrön, M., Ingwersen, J., Oswald, S., 2018. Uncertainty, sensitivity and improvements in soil moisture estimation with cosmic-ray neutron sensing. J. Hydrol. 564, 873–887.

Bauer-Marschallinger, B., Freeman, V., Cao, S., Paulik, C., Schaufler, S., Stachl, T., Modanesi, S., Massari, C., Ciabatta, L., Brocca, L.L., Wagner, W., 2019. Toward global soil moisture monitoring with sentinel-1: harnessing assets and overcoming obstacles. IEEE Trans. Geosci. Rem. Sens. 57, 520–539.

Bayat, A.T., Schönbrodt-Stitt, S., Nasta, P., Ahmadian, N., Conrad, C., Bogena, H.R., Vereecken, H., Jakobi, J., Baatz, R., Romano, N., 2020. Mapping near-surface soil moisture in a mediterranean agroforestry ecosystem using cosmic-ray neutron probe and sentinel-1 data. In: 2020 IEEE International Workshop on Metrology for Agriculture and Forestry (MetroAgriFor). IEEE, pp. 201–206.

Bayerisches Landesamt für Umwelt, 2014. Übersichtsbodenkarte tk25-blatt 8132. www.lfu.bayern.de.

Beale, J., Snapir, B., Waine, T., Evans, J., Corstanje, R., 2019. The significance of soil properties to the estimation of soil moisture from c-band synthetic aperture radar. Hydrol. Earth Syst. Sci. Discuss. 1–32.

Beven, K.J., Kirkby, M.J., 1979. A physically based, variable contributing area model of basin hydrology. Hydrol. Sci. Bull. 24 (1), 43–69.
Bollig, C., Feller, U., 2014. Impacts of drought stress on water relations and carbon assimilation in grassland species at different altitudes. Agric. Ecosyst. Environ. 188, 212–220.
Breiman, L., 2001. Random forests. Mach. Learn. 45 (1), 5–32.
Burke, I.C., Lauenroth, W.K., Vinton, M.A., Hook, P.B., Kelly, R.H., Epstein, H.E., Aguiar, M.R., Robles, M.D., Aguilera, M.O., Murphy, K.L., et al., 1998. Plant-soil interactions in temperate grasslands. In: Plant-induced Soil Changes: Processes and Feedbacks. Springer, pp. 121–143.
Carlson, T.N., Perry, E.M., Schmugge, T.J., 1990. Remote estimation of soil moisture availability and fractional vegetation cover for agricultural fields. Agric. For. Meteorol. 52 (1–2), 45–69.
Crow, W.T., Ryu, D., Famiglietti, J.S., 2005. Upscaling of field-scale soil moisture measurements using distributed land surface modeling. Adv. Water Resour. 28 (1), 1–14.
Daughtry, C.S., Walthall, C., Kim, M., De Colstoun, E.B., McMurtrey Iii, J., 2000. Estimating corn leaf chlorophyll concentration from leaf and canopy reflectance. Rem. Sens. Environ. 74 (2), 229–239.
Desilets, D., Zreda, M., Ferré, T.P., 2010. Nature's neutron probe: land surface hydrology at an elusive scale with cosmic rays. Water Resour. Res. 46 (11).
Dimitrova-Petrova, K., Geris, J., Wilkinson, M.E., Rosolem, R., Verrot, L., Lilly, A., Soulsby, C., 2020. Opportunities and challenges in using catchment-scale storage estimates from cosmic ray neutron sensors for rainfall-runoff modelling. J. Hydrol. 586, 124878.
Döpper, Veronika, Duarte Rocha, Alby, Berger, Katja, Gränzig, Tobias, Verrelst, Jochem, Kleinschmit, Birgit, Förster, Michael, 2022. Estimating soil moisture content under grassland with hyperspectral data using radiative transfer modelling and machine learning. Int. J. Appl. Earth Obs. Geoinf.
Duygu, M.B., Akyürek, Z., 2019. Using cosmic-ray neutron probes in validating satellite soil moisture products and land surface models. Water 11 (7), 1362.
Edokossi, K., Calabia, A., Jin, S., Molina, I., 2020. Gnss-reflectometry and remote sensing of soil moisture: a review of measurement techniques, methods, and applications. Rem. Sens. 12 (4). URL. https://www.mdpi.com/2072-4292/12/4/614.
El Hajj, M., Baghdadi, N., Bazzi, H., Zribi, M., 2019. Penetration analysis of sar signals in the c and l bands for wheat, maize, and grasslands. Rem. Sens. 11 (1), 31.
El Hajj, M., Baghdadi, N., Zribi, M., Bazzi, H., 2017. Synergic use of sentinel-1 and sentinel-2 images for operational soil moisture mapping at high spatial resolution over agricultural areas. Rem. Sens. 9 (12).
Engman, E.T., Chauhan, N., 1995. Status of microwave soil moisture measurements with remote sensing. Remote Sens. Environ. 51 (1), 189–198.
Esch, S., 2018. Determination of soil moisture and vegetation parameters from spaceborne c-band sar on agricultural areas. Ph.D. thesis, Universität zu Köln.
Fairfield, J., Leymarie, P., 1991. Drainage networks from grid digital elevation models. Water Resour. Res. 27 (5), 709–717.
Fersch, B., Francke, T., Heistermann, M., Schrön, M., Döpper, V., Jakobi, J., 2020a. A Massive Coverage Experiment of Cosmic Ray Neutron Sensors for Soil Moisture Observation in a Pre-alpine Catchment in Se-germany (Part I: Core Data) [post-Review Version].
Fersch, B., Francke, T., Heistermann, M., Schrön, M., Döpper, V., Jakobi, J., Baroni, G., Blume, T., Bogena, H., Budach, C., et al., 2020b. A dense network of cosmic-ray neutron sensors for soil moisture observation in a highly instrumented pre-alpine headwater catchment in Germany. Earth Syst. Sci. Data 12 (3), 2289–2309.
Fersch, B., Jagdhuber, T., Schrön, M., Völksch, I., Jäger, M., 2018. Synergies for soil moisture retrieval across scales from airborne polarimetric sar, cosmic ray neutron roving, and an in situ sensor network. Water Resour. Res. 54 (11), 9364–9383.
Fort, F., Volaire, F., Guilioni, L., Barkaoui, K., Navas, M.-L., Roumet, C., 2017. Root traits are related to plant water-use among rangeland mediterranean species. Funct. Ecol. 31 (9), 1700–1709.
Franz, T.E., Wahbi, A., Zhang, J., Vreugdenhil, M., Heng, L., Dercon, G., Strauss, P., Brocca, L., Wagner, W., 2020. Practical data products from cosmic-ray neutron sensing for hydrological applications. Front. Water 2, 9.
Ghajarnia, N., Kalantari, Z., Orth, R., Destouni, G., 2020. Close co-variation between soil moisture and runoff emerging from multi-catchment data across europe. Sci. Rep. 10 (1), 1–11.
Grayson, R.B., Western, A.W., Chiew, F.H., Blöschl, G., 1997. Preferred states in spatial soil moisture patterns: local and nonlocal controls. Water Resour. Res. 33 (12), 2897–2908.
Gross, N., Robson, T., Lavorel, S., Albert, C., Le Bagousse-Pinguet, Y., Guillemin, R., 2008. Plant response traits mediate the effects of subalpine grasslands on soil moisture. New Phytol. 180 (3), 652–662.
Gruber, A., De Lannoy, G., Albergel, C., Al-Yaari, A., Brocca, L., Calvet, J.-C., Colliander, A., Cosh, M., Crow, W., Dorigo, W., Draper, C., Hirschi, M., Kerr, Y., Konings, A., Lahoz, W., McColl, K., Montzka, C., Muñoz-Sabater, J., Peng, J., Reichle, R., Richaume, P., Rüdiger, C., Scanlon, T., van der Schalie, R., Wigneron, J.-P., Wagner, W., 2020. Validation practices for satellite soil moisture retrievals: what are (the) errors? Remote Sens. Environ. 244, 111806.
Guderle, M., Bachmann, D., Milcu, A., Gockele, A., Bechmann, M., Fischer, C., Roscher, C., Landais, D., Ravel, O., Devidal, S., Roy, J., Gessler, A., Buchmann, N., Weigelt, A., Hildebrandt, A., 2018. Dynamic niche partitioning in root water uptake facilitates efficient water use in more diverse grassland plant communities. Funct. Ecol. 32 (1), 214–227.
Haboudane, D., Miller, J.R., Tremblay, N., Zarco-Tejada, P.J., Dextraze, L., 2002. Integrated narrow-band vegetation indices for prediction of crop chlorophyll content for application to precision agriculture. Remote Sens. Environ. 81 (2), 416–426.
Hänsch, R., Jagdhuber, T., Fersch, B., 2020. Soil-permittivity estimation under grassland using machine-learning and polarimetric decomposition techniques. IEEE Trans. Geosci. Rem. Sens. 1–11.
Hardisky, M., Klemas, V., Smart, a., 01 1983. The influence of soil salinity, growth form, and leaf moisture on the spectral radiance of spartina alterniflora canopies. Photogramm. Eng. Rem. Sens. 48, 77–84.
Hassan-Esfahani, L., Torres-Rua, A., Jensen, A., Mckee, M., 2017. Spatial root zone soil water content estimation in agricultural lands using bayesian-based artificial neural networks and high-resolution visual, nir, and thermal imagery. Irrigat. Drain. 66 (2), 273–288.
Haubrock, S., Chabrillat, S., Lemmnitz, C., Kaufmann, H., 2008. Surface soil moisture quantification models from reflectance data under field conditions. Int. J. Rem. Sens. 29 (1), 3–29.
Heistermann, M., Francke, T., Schrön, M., Oswald, S.E., 2021. Spatio-temporal soil moisture retrieval at the catchment-scale using a dense network of cosmic-ray neutron sensors. Hydrol. Earth Syst. Sci. Discuss. 2021, 1–35.
Hildebrandt, A., 2020. Root-water relations and interactions in mixed forest settings. In: Levia, D.F., Carlyle-Moses, D.E., Iida, S., Michalzik, B., Nanko, K., Tischer, A. (Eds.), Forest-water Interactions. Springer International Publishing, Cham, pp. 319–348.
Holtgrave, A.-K., Förster, M., Greifeneder, F., Notarnicola, C., Kleinschmit, B., 2018. Estimation of soil moisture in vegetation-covered floodplains with sentinel-1 sar data using support vector regression. PFG–Journal of Photogrammetry, Remote Sens. Geoinf. Sci. 86 (2), 85–101.
Holtgrave, A.-K., Röder, N., Ackermann, A., Erasmi, S., Kleinschmit, B., 2020. Comparing sentinel-1 and-2 data and indices for agricultural land use monitoring. Rem. Sens. 12 (18), 2919.
Holzman, M.E., Carmona, F., Rivas, R., Niclòs, R., 2018. Early assessment of crop yield from remotely sensed water stress and solar radiation data. ISPRS J. Photogrammetry Remote Sens. 145, 297–308.
Horn, B.K.P., 1981. Hill shading and the reflectance map. Proc. IEEE 69 (1), 14–47.
Howells, O.D., Petropoulos, G.P., Srivastava, P.K., Triantakonstantis, D., Sandric, I., 2021. Exploring the potential of SCAT-SAR SWI for soil moisture retrievals at selected COSMOS-UK sites. Int. J. Rem. Sens. 42 (23), 9155–9169. https://doi.org/10.1080/01431161.2021.1988185 publisher: Taylor & Francis _eprint: https://doi.org/10.1080/01431161.2021.1988185.
Huete, A., 1988. A soil-adjusted vegetation index (savi). Remote Sens. Environ. 25 (3), 295–309.
Huete, A.R., Justice, C., van Leeuwen, W., 1996. MODIS Vegetation Index (MOD 13), EOS MODIS Algorithm-Theoretical Basis Document. NASA Goddard Space Flight Center.
Iwema, J., Schrön, M., Koltermann Da Silva, J., Schweiser De Paiva Lopes, R., Rosolem, R., 2021. Accuracy and precision of the cosmic-ray neutron sensor for soil moisture estimation at humid environments. Hydrol. Process. 35 (11), e14419.
Jagdhuber, T., 2012. Soil Parameter Retrieval under Vegetation Cover Using Sar Polarimetry. Ph.D. thesis, RIMAX Publications, RIMAX, Deutsches GeoForschungsZentrum.
Jakobi, J., Huisman, J., Vereecken, H., Diekkrüger, B., Bogena, H., 2018. Cosmic ray neutron sensing for simultaneous soil water content and biomass quantification in drought conditions. Water Resour. Res. 54 (10), 7383–7402.
Kiese, R., Fersch, B., Baessler, C., Brosy, C., Butterbach-Bahl, K., Chwala, C., Dannenmann, M., Fu, J., Gasche, R., Grote, R., et al., 2018. The tereno pre-alpine observatory: integrating meteorological, hydrological, and biogeochemical measurements and modeling. Vadose Zone J. 17 (1), 1–17.
Köhli, M., Schrön, M., Zreda, M., Schmidt, U., Dietrich, P., Zacharias, S., 2015. Footprint characteristics revised for field-scale soil moisture monitoring with cosmic-ray neutrons. Water Resour. Res. 51 (7), 5772–5790.
Köhli, M., Weimar, J., Schrön, M., Baatz, R., Schmidt, U., 2021. Soil moisture and air humidity dependence of the above-ground cosmic-ray neutron intensity. Front. Water 2, 66.
Korres, W., Koyama, C., Fiener, P., Schneider, K., 2010. Analysis of surface soil moisture patterns in agricultural landscapes using empirical orthogonal functions. Hydrol. Earth Syst. Sci. 14 (5), 751–764.
Kumar, K.A., Setia, R., Pandey, D.K., Putrevu, D., Misra, A., Pateriya, B., 2021. Soil moisture retrieval techniques using satellite remote sensing. In: Mitran, T., Meena, R. S., Chakraborty, A. (Eds.), Geospatial Technologies for Crops and Soils. Springer Singapore, Singapore, pp. 357–385.
Landesamt für Digitalisierung, 2009. Breitband und Vermessung. Dgm1. https://www.ldbv.bayern.de/produkte/3dprodukte/gelaende.html.
Landesamt für Digitalisierung, 2018. Breitband und Vermessung. Bodenschätzung. https://geoservices.bayern.de/wms/v1/ogc_alkis_bosch.cgi?.
Lei, J., Yang, W., Yang, X., Jan. 2022. Soil moisture in a vegetation-covered area using the improved water cloud model based on remote sensing. J. Indian Soc. Remote Sens. 50 (1), 1–11. https://doi.org/10.1007/s12524-021-01450-2. URL.
Li, Z.-L., Leng, P., Zhou, C., Chen, K.-S., Zhou, F.-C., Shang, G.-F., 2021. Soil moisture retrieval from remote sensing measurements: current knowledge and directions for the future. Earth Sci. Rev. 218, 103673. URL. https://www.sciencedirect.com/science/article/pii/S0012825221001744.
Liu, S., Roberts, D.A., Chadwick, O.A., Still, C.J., 2012. Spectral responses to plant available soil moisture in a californian grassland. Int. J. Appl. Earth Obs. Geoinf. 19, 31–44.
Liu, Y., Qian, J., Yue, H., 2020. Combined sentinel-1a with sentinel-2a to estimate soil moisture in farmland. IEEE J. Sel. Top. Appl. Earth Obs. Rem. Sens.
Liu, Y., Qian, J., Yue, H., 2021. Comprehensive evaluation of sentinel-2 red edge and shortwave-infrared bands to estimate soil moisture. IEEE J. Sel. Top. Appl. Earth Obs. Rem. Sens. 14, 7448–7465.

Lu, Z., Peng, S., Slette, I., Cheng, G., Li, X., Chen, A., Jan. 2021. Soil moisture seasonality alters vegetation response to drought in the Mongolian Plateau. Environ. Res. Lett. 16 (1), 014050 https://doi.org/10.1088/1748-9326/abd1a2 publisher: IOP Publishing. URL.
Ma, C., Li, X., McCabe, M., 07 2020. Retrieval of high-resolution soil moisture through combination of sentinel-1 and sentinel-2 data. Rem. Sens. 12, 2303.
Massari, C., Camici, S., Ciabatta, L., Brocca, L., 2018. Exploiting satellite-based surface soil moisture for flood forecasting in the mediterranean area: state update versus rainfall correction. Rem. Sens. 10 (2), 292.
McFeeters, S.K., 1996. The use of the normalized difference water index (ndwi) in the delineation of open water features. Int. J. Rem. Sens. 17 (7), 1425–1432.
Mengen, D., Montzka, C., Jagdhuber, T., Fluhrer, A., Brogi, C., Baum, S., Schüttemeyer, D., Bayat, B., Bogena, H., Coccia, A., Masalias, G., Trinkel, V., Jakobi, J., Jonard, F., Ma, Y., Mattia, F., Palmisano, D., Rascher, U., Satalino, G., Schumacher, M., Koyama, C., Schmidt, M., Vereecken, H., 2021. The sarsense campaign: air- and space-borne c- and l-band sar for the analysis of soil and plant parameters in agriculture. Rem. Sens. 13 (4).
Mohanty, B.P., Cosh, M.H., Lakshmi, V., Montzka, C., 2017. Soil moisture remote sensing: state-of-the-science. Vadose Zone J. 16 (1), 1–9.
Montzka, C., Bogena, H.R., Zreda, M., Monerris, A., Morrison, R., Muddu, S., Vereecken, H., 2017. Validation of spaceborne and modelled surface soil moisture products with cosmic-ray neutron probes. Rem. Sens. 9 (2), 103.
Naithani, K.J., Baldwin, D.C., Gaines, K.P., Lin, H., Eissenstat, D.M., 2013. Spatial distribution of tree species governs the spatio-temporal interaction of leaf area index and soil moisture across a forested landscape. PLoS One 8 (3), e58704.
Nasirzadehdizaji, R., Balik Sanli, F., Abdikan, S., Cakir, Z., Sekertekin, A., Ustuner, M., 2019. Sensitivity analysis of multi-temporal sentinel-1 sar parameters to crop height and canopy coverage. Appl. Sci. 9 (4), 655.
Neutron Monitor Database, 2019. Jung. http://www.nmdb.eu.
Nippert, J.B., Knapp, A.K., 2007. Linking water uptake with rooting patterns in grassland species. Oecologia 153 (2), 261–272.
Nolan, M., Fatland, D.R., 2003. Penetration depth as a dinsar observable and proxy for soil moisture. IEEE Trans. Geosci. Rem. Sens. 41 (3), 532–537.
Ottosen, T.-B., Petch, G., Hanson, M., SkjÃ, th C.A., 2020. Tree cover mapping based on sentinel-2 images demonstrate high thematic accuracy in europe. Int. J. Appl. Earth Obs. Geoinf. 84, 101947.
Owe, M., Van de Griend, A.A., 1998. Comparison of soil moisture penetration depths for several bare soils at two microwave frequencies and implications for remote sensing. Water Resour. Res. 34 (9), 2319–2327.
Paloscia, S., Pettinato, S., Santi, E., Notarnicola, C., Pasolli, L., Reppucci, A., 2013. Soil moisture mapping using sentinel-1 images: algorithm and preliminary validation. Remote Sens. Environ. 134, 234–248.
Pasolli, L., Notarnicola, C., Bertoldi, G., Bruzzone, L., Remelgado, R., Greifeneder, F., Niedrist, G., Della Chiesa, S., Tappeiner, U., Zebisch, M., 2015. Estimation of soil moisture in mountain areas using svr technique applied to multiscale active radar images at c-band. IEEE J. Sel. Top. Appl. Earth Obs. Rem. Sens. 8 (1), 262–283.
Pasolli, L., Notarnicola, C., Bertoldi, G., Della Chiesa, S., Niedrist, G., Bruzzone, L., Tappeiner, U., Zebisch, M., 2014. Soil moisture monitoring in mountain areas by using high-resolution sar images: results from a feasibility study. Eur. J. Soil Sci. 65 (6), 852–864.
Patil, A., Fersch, B., Hendricks Franssen, H.-J., Kunstmann, H., 2021. Assimilation of cosmogenic neutron counts for improved soil moisture prediction in a distributed land surface model. Front. Water 3. URL. https://www.frontiersin.org/article/10.3389/frwa.2021.729592.
Pearson, R.L., Miller, L.D., 1972. Remote mapping of standing crop biomass for estimation of the productivity of the shortgrass prairie. Remote Sens. Environ. VIII, 1355.
Pedregosa, F., Varoquaux, G., Gramfort, A., Michel, V., Thirion, B., Grisel, O., Blondel, M., Prettenhofer, P., Weiss, R., Dubourg, V., Vanderplas, J., Passos, A., Cournapeau, D., Brucher, M., Perrot, M., Duchesnay, E., 2011. Scikit-learn: machine learning in Python. J. Mach. Learn. Res. 12, 2825–2830.
Peng, C., Deng, M., Di, L., 2014. Relationships between remote-sensing-based agricultural drought indicators and root zone soil moisture: a comparative study of Iowa. IEEE J. Sel. Top. Appl. Earth Obs. Rem. Sens. 7 (11), 4572–4580.
Peng, J., Albergel, C., Balenzano, A., Brocca, L., Cartus, O., Cosh, M.H., Crow, W.T., Dabrowska-Zielinska, K., Dadson, S., Davidson, M.W., de Rosnay, P., Dorigo, W., Gruber, A., Hagemann, S., Hirschi, M., Kerr, Y.H., Lovergine, F., Mahecha, M.D., Marzahn, P., Mattia, F., Musial, J.P., Preuschmann, S., Reichle, R.H., Satalino, G., Silgram, M., van Bodegom, P.M., Verhoest, N.E., Wagner, W., Walker, J.P., Wegmüller, U., Loew, A., 2021. A roadmap for high-resolution satellite soil moisture applications - confronting product characteristics with user requirements. Remote Sens. Environ. 252, 112162.
Porporato, A., Laio, F., Ridolfi, L., Rodriguez-Iturbe, I., 2001. Plants in water-controlled ecosystems: active role in hydrologic processes and response to water stress: iii. vegetation water stress. Adv. Water Resour. 24 (7), 725–744.
Power, D., Rico-Ramirez, M.A., Desilets, S., Desilets, D., Rosolem, R., 2021. Cosmic-Ray neutron Sensor PYthon tool (crspy 1.2.1): an open-source tool for the processing of cosmic-ray neutron and soil moisture data. Geosci. Model Dev. (GMD) 14 (12), 7287–7307. URL. https://gmd.copernicus.org/articles/14/7287/2021/.
Qi, J., Chehbouni, A., Huete, A., Kerr, Y., Sorooshian, S., 1994. A modified soil adjusted vegetation index. Remote Sens. Environ. 48 (2), 119–126.
Riedel, T., Pathe, C., Thiel, C., Herold, M., Schmullius, C., 2002. Systematic investigation on the effect of dew and interception on multifrequency and multipolarimetric radar backscatter signals. In: Retrieval of Bio-and Geo-Physical Parameters from SAR Data for Land Applications, 475, pp. 99–104.
Robinson, D., Campbell, C., Hopmans, J., Hornbuckle, B.K., Jones, S.B., Knight, R., Ogden, F., Selker, J., Wendroth, O., 2008. Soil moisture measurement for ecological and hydrological watershed-scale observatories: a review. Vadose Zone J. 7 (1), 358–389.
Rock, B.N., Vogelmann, J.E., Williams, D.L., Vogelmann, A.F., Hoshizaki, T., 1986. Remote detection of forest damage. Bioscience 36 (7), 439–445.
Rosenbaum, U., Bogena, H.R., Herbst, M., Huisman, J., Peterson, T., Weuthen, A., Western, A., Vereecken, H., 2012. Seasonal and event dynamics of spatial soil moisture patterns at the small catchment scale. Water Resour. Res. 48 (10).
Rouse, J.W., Haas, R.H., Schell, J.A., Deering, D.W., Harlan, J.C., 1974. Monitoring the Vernal Advancement of Retrogradation of Natural Vegetation. NASA/GSFC.
Rujoiu-Mare, M.-R., Olariu, B., Mihai, B.-A., Nistor, C., Săvulescu, I., 2017. Land cover classification in Romanian carpathians and subcarpathians using multi-date sentinel-2 remote sensing imagery. Eur. J. Remote Sens. 50 (1), 496–508.
Saatchi, S., 2019. Sar methods for mapping and monitoring forest biomass. In: Flores, A., Herndon, K., Thapa, R., Cherrington, E. (Eds.), SAR Handbook: Comprehensive Methodologies for Forest Monitoring and Biomass Estimation. NASA.
Sadeghi, M., Babaeian, E., Tuller, M., Jones, S.B., 2017. The optical trapezoid model: a novel approach to remote sensing of soil moisture applied to sentinel-2 and landsat-8 observations. Remote Sens. Environ. 198, 52–68.
Sánchez-Espinosa, A., Schröder, C., 2019. Land use and land cover mapping in wetlands one step closer to the ground: sentinel-2 versus landsat 8. J. Environ. Manag. 247, 484–498.
Scheiffele, L.M., Baroni, G., Franz, T.E., Jakobi, J., Oswald, S.E., 2020. A profile shape correction to reduce the vertical sensitivity of cosmic-ray neutron sensing of soil moisture. Vadose Zone J. 19 (1), e20083. _eprint: https://acsess.onlinelibrary.wiley.com/doi/pdf/10.1002/vzj2.20083.
Schnur, M.T., Xie, H., Wang, X., 2010. Estimating root zone soil moisture at distant sites using modis ndvi and evi in a semi-arid region of southwestern USA. Ecol. Inf. 5 (5), 400–409.
Schrön, M., Oswald, S.E., Zacharias, S., Kasner, M., Dietrich, P., Attinger, S., 2021. Neutrons on rails: transregional monitoring of soil moisture and snow water equivalent. Geophys. Res. Lett. 48 (24), e2021GL093924. _eprint: https://agupubs.onlinelibrary.wiley.com/doi/pdf/10.1029/2021GL093924.
Schrön, M., Köhli, M., Scheiffele, L., Iwema, J., Bogena, H.R., Lv, L., Martini, E., Baroni, G., Rosolem, R., Weimar, J., et al., 2017. Improving calibration and validation of cosmic-ray neutron sensors in the light of spatial sensitivity. Hydrol. Earth Syst. Sci. 21 (10), 5009–5030.
Schrön, M., Rosolem, R., Köhli, M., Piussi, L., Schröter, I., Iwema, J., Kögler, S., Oswald, S., Wollschläger, U., Samaniego, L., et al., 2018. Cosmic-ray neutron rover surveys of field soil moisture and the influence of roads. Water Resour. Res. 54 (9), 6441–6459.
Schröter, I., Paasche, H., Dietrich, P., Wollschläger, U., 2015. Estimation of catchment-scale soil moisture patterns based on terrain data and sparse tdr measurements using a fuzzy c-means clustering approach. Vadose Zone J. 14 (11) vzj2015.01.0008.
Sedaghat, A., Shahrestani, M.S., Noroozi, A.A., Fallah Nosratabad, A., Bayat, H., 2022. Developing pedotransfer functions using sentinel-2 satellite spectral indices and machine learning for estimating the surface soil moisture. J. Hydrol. 606, 127423. URL. https://www.sciencedirect.com/science/article/pii/S0022169421014736.
Shih, S.F., Jordan, J.D., 1992. Landsat mid-infrared data and gis in regional surface soil-moisture assessment 1. JAWRA J. Am. Water Resour. Assoc. 28 (4), 713–719.
Sims, D., Gamon, J., 08 2002. Relationships between leaf pigment content and spectral reflectance across a wide range of species, leaf structures and developmental stages. Remote Sens. Environ. 81, 337–354.
Sobrino, J., Franch, B., Mattar, C., Jiménez-Muñoz, J., Corbari, C., 2012. A method to estimate soil moisture from airborne hyperspectral scanner (ahs) and aster data: application to sen2flex and sen3exp campaigns. Remote Sens. Environ. 117, 415–428.
Stockmann, I., 2020. Biomasseschätzung in einem temperierten Mischwald auf der Basis von Höheninformationen und multitemporalen RapidEye Daten. University of Potsdam, Potsdam, Germany.
Ulaby, F., Long, D., Blackwell, W., Elachi, C., Fung, A., Ruf, C., Sarabandi, K., Zyl, J., Zebker, H., 01, 2014. Microwave Radar and Radiometric Remote Sensing. University of Michigan Press.
Veloso, A., Mermoz, S., Bouvet, A., Le Toan, T., Planells, M., Dejoux, J.-F., Ceschia, E., 2017. Understanding the temporal behavior of crops using sentinel-1 and sentinel-2-like data for agricultural applications. Remote Sens. Environ. 199, 415–426.
Vereecken, H., Kasteel, R., Vanderborght, J., Harter, T., 2007. Upscaling hydraulic properties and soil water flow processes in heterogeneous soils: a review. Vadose Zone J. 6 (1), 1–28.
Vergopolan, N., Chaney, N.W., Pan, M., Sheffield, J., Beck, H.E., Ferguson, C.R., Torres-Rojas, L., Sadri, S., Wood, E.F., 2021. Smap-hydroblocks, a 30-m satellite-based soil moisture dataset for the conterminous us. Sci. Data 8 (1), 1–11.
Vinnikov, K.Y., Robock, A., Speranskaya, N.A., Schlosser, C.A., 1996. Scales of temporal and spatial variability of midlatitude soil moisture. J. Geophys. Res. Atmos. 101 (D3), 7163–7174.
Wang, L., Qu, J.J., 2007. Nmdi: a normalized multi-band drought index for monitoring soil and vegetation moisture with satellite remote sensing. Geophys. Res. Lett. 34 (20).
Wang, S., Fu, B.-J., Gao, G., Yao, X., Zhou, J., 08 2012. Soil moisture and evapotranspiration of different land cover types in the loess plateau, China. Hydrol. Earth Syst. Sci. 16, 2883–2892.
West, H., Quinn, N., Horswell, M., White, P., 2018. Assessing vegetation response to soil moisture fluctuation under extreme drought using sentinel-2. Water 10 (7), 838.
Western, A.W., Blöschl, G., Grayson, R.B., 1998. Geostatistical characterisation of soil moisture patterns in the tarrawarra catchment. J. Hydrol. 205 (1–2), 20–37.

Wyatt, B.M., Ochsner, T.E., Zou, C.B., 2021. Estimating root zone soil moisture across diverse land cover types by integrating in-situ and remotely sensed data. Agric. For. Meteorol. 307, 108471. URL. https://www.sciencedirect.com/science/article/pii/S0168192321001544.

Xie, Q., Dash, J., Huete, A., Jiang, A., Yin, G., Ding, Y., Peng, D., Hall, C.C., Brown, L., Shi, Y., Ye, H., Dong, Y., Huang, W., 2019. Retrieval of crop biophysical parameters from Sentinel-2 remote sensing imagery. Int. J. Appl. Earth Obs. Geoinf. 80, 187–195. URL. https://www.sciencedirect.com/science/article/pii/S0303243419301199.

Yang, L., Sun, G., Zhi, L., Zhao, J., 2018. Negative soil moisture-precipitation feedback in dry and wet regions. Sci. Rep. 8 (1), 1–9.

Zaman, B., McKee, M., Neale, C.M., 2012. Fusion of remotely sensed data for soil moisture estimation using relevance vector and support vector machines. Int. J. Rem. Sens. 33 (20), 6516–6552.

Zevenbergen, L.W., Thorne, C.R., 1987. Quantitative analysis of land surface topography. Earth Surf. Process. Landforms 12 (1), 47–56.

Zhang, C., Pattey, E., Liu, J., Cai, H., Shang, J., Dong, T., 2018. Retrieving leaf and canopy water content of winter wheat using vegetation water indices. IEEE J. Sel. Top. Appl. Earth Obs. Rem. Sens. 11 (1), 112–126.

Zhang, D., Zhou, G., 2016. Estimation of soil moisture from optical and thermal remote sensing: a review. Sensors 16 (8), 1308.

Zhao, C., Qin, Q., 2019. A physically-based model for canopy water content retrieval. In: IGARSS 2019 - 2019 IEEE International Geoscience and Remote Sensing Symposium, pp. 6122–6125.

Zreda, M., Desilets, D., Ferré, T.P.A., Scott, R.L., 2008. Measuring soil moisture content non-invasively at intermediate spatial scale using cosmic-ray neutrons. Geophys. Res. Lett. 35 (21).